Dalton Transactions

Accepted Manuscript

This article can be cited before page numbers have been issued, to do this please use: S. Eady, T. Breault, L. Thompson and N. Lehnert, *Dalton Trans.*, 2015, DOI: 10.1039/C5DT03744A.

ROYAL SOCIETY OF CHEMISTRY

www.rsc.org/dalton

View Article Online
DOI: 10.1039/C5DT03744A

Highly Functionalizable Penta-Coordinate Iron Hydrogen Production Catalysts with Low Overpotentials

Shawn C. Eady[†], *Tanya Breault*[‡], *Levi Thompson*[‡], *Nicolai Lehnert*[†*]

[†]Department of Chemistry, University of Michigan, 930 North University, Ann Arbor, Michigan 48109-1055, United States

[‡]Department of Chemical Engineering, University of Michigan, 1221 Beal Avenue, Ann Arbor, Michigan 48109-2102, United States

KEYWORDS: Sustainable Chemistry, Electrocatalysis, Hydrogen Fuel

ABSTRACT Penta-coordinate iron carbonyl complexes that are built around the rigid Fe(PNP) motif (PNP = $(C_6H_5)_2PN(R)P(C_6H_5)_2$) are synthesized and structurally and spectroscopically characterized. These complexes allow for facile customization of the secondary ligand sphere with various types of linkers and functional groups. The new $[Fe(S_2C_6H_4)(PNP)(CO)]$ complexes show dihydrogen production electrocatalysis at overpotentials of 0.09-0.21 V vs. Pt under mildly acidic conditions (and activities from 0.28 to 3.51 s^{-1}). The most active compound exhibits a turnover frequency (TOF) of 3.51 s^{-1} at an overpotential of only 0.15 V vs. Pt. Trends in activity are further analyzed. It is found that (a) a decrease in overpotential correlates strongly with the electron withdrawing strength of the PNP amine substituent, and (b) aliphatic substituents give comparatively higher TOFs than aromatic ones. An EC-type mechanism is shown to proceed by initial reduction of the Fe^{II} metal center and proposed formation of an Fe^{III} hydride intermediate. Analogous cobalt compounds were synthesized and characterized, but were found to have low

View Article Online
DOI: 10.1039/C5DT03744A

stability in acidic media under turnover conditions, and hence, are unsuitable as catalysts for proton reduction.

Introduction

The search for sustainable dihydrogen production systems has been an ongoing focus of global research efforts for nearly half a century.[1-3] Incorporation of non-precious metal catalysts to yield efficient dihydrogen production manifolds in aqueous systems is an ever-growing area in the field of electrocatalysis.[4,5] Major discoveries in proton reduction electrochemistry have been made in the past few decades, which suggests that non-precious metals such as iron, nickel and cobalt with selected ligand manifolds and the correct environment may provide activities and stabilities competitive to platinum and similar rare metal catalysts.[6-23 11,24-41]

A major challenge in the design of industrially viable electrocatalysts is minimizing the wasted input energy, i.e. overpotential, required for catalyst activation. A number of iron- and nickel-centered electrocatalysts for dihydrogen production with incredible activities (>10,000 s^{-1}) have been reported in the literature; however, many of these are only active in strongly acidic conditions or have moderate to high overpotentials, typically in excess of 200 mV.[6,42] It is therefore the focus of this study to investigate catalytic systems capable of functioning in weakly acidic media with minimal overpotentials.

In addition, to transition from basic scientific research in catalyst development to application-driven research, easy access to a variety of functionalities in the ligand periphery of a catalyst is desirable.[43-45] One such application is the heterogenization of catalysts via immobilization on electrode surfaces, especially in light-driven proton reduction systems that couple water

View Article Online
DOI: 10.1039/C5DT03744A

oxidation with proton reduction for efficient water splitting.[12,29,41,44-51] Realization of such systems is met with formidable obstacles, including a means of providing a versatile ligand system that will not impact catalyst 'core' structure and function upon derivatization and surface immobilization. Thus it can be reasoned that the development of suitable strategies and ligand systems for catalyst immobilization is as important as the catalyst design itself, and having a catalyst system with an easily customizable ligand periphery is critical for future applications.

Previously, penta-coordinate iron catalysts that are active for proton reduction have been reported by Ott and coworkers.[37] These compounds display impressive activity (TOF > 500 s^{-1}) with modest overpotentials (0.17-0.24 V vs. Pt for acetic acid concentrations of 0.1-0.5 M, respectively) and were obtained in high yields in a single synthetic step from diphosphine and dithiolate ligands under atmospheric CO pressure. However, these complexes utilize a conformationally flexible diphosphine ligand, which, when locked into a fixed conformation in the surface-bound state, might become less active.[44] Herein we report catalytically active derivatives with a much more rigid, conjugated 'PNP' ligand structure, leading to iron complexes that contain a very rigid, Fe-P-N-P four-membered ring. Several derivatives of these complexes are presented and are characterized structurally as well as spectroscopically. Electrochemical properties of the complexes are further investigated, in addition to their activities for proton reduction. These systems provide a versatile, yet simple 'toolbox' for ligand derivatization which can be tailored to a variety of applications.

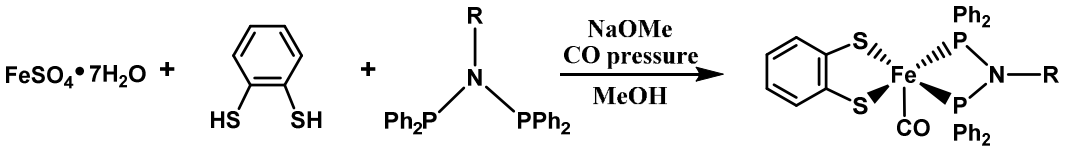

Scheme 1. Preparation of penta-coordinate iron dihydrogen production catalysts.

Experimental Section

View Article Online
DOI: 10.1039/C5DT03744A

General Procedures

Unless otherwise stated, all syntheses were performed under a dinitrogen atmosphere with distilled and degassed solvents.

Materials. Isopropylamine (99%), triethylamine (>99%), 1-amino-3-aminobutyne (95%), 1-pyrenemethylamine hydrochloride (95%), 1-pyrenebutanol (99%), aniline (99%), 4-bromoaniline (97%), 4-fluoroaniline (99%), 4-fluorobenzylamine (97%), 4-phenylbutylamine (97%), benzene-1,2-dithiol (97%), toluene-3,4-dithiol (>97%), and 3,6-dichloro-1,2-benzenedithiol (95%), and Fe(II) sulfate heptahydrate (>99%) were all purchased from Sigma Aldrich and used as received. Methylene chloride, acetonitrile and hexane were all purchased from Fisher (ACS grade), distilled over calcium hydride, and degassed with a dinitrogen purge before use. Methanol was purchased from Fisher (ACS grade), distilled over magnesium sulfate (Fisher), and degassed with dinitrogen prior to use.

Physical Measurements. ^{1}H NMR spectra at 500 MHz, ^{31}P NMR spectra at 202 and ^{19}F NMR spectra at 348 MHz were obtained on a Bruker DMX 400 spectrometer. All ^{1}H chemical shifts were measured relative to residual protons in the lock solvents and are referenced to Me_4Si (0.00 ppm). ^{31}P NMR chemical shifts are referenced to the corresponding proton experiment conducted directly prior to the ^{31}P measurement. ^{19}F chemical shifts were referenced to a CCl_3F internal standard set to 0 ppm. All mass spectra collected using electrospray ionization (ESI) techniques were recorded on a Micromass Autospec Spectrometer Premier. Solid state infrared (IR) spectra were recorded on a Perkin Elmer Spectrum 100 FT-IR spectrometer by embedding the compounds in a KBr matrix. Solution IR studies were conducted in acetonitrile (purified as described above) and measurements were performed between NaCl plates. Elemental analyses were performed by Atlantic Microlab, Inc, Norcross, GA.

View Article Online
DOI: 10.1039/C5DT03744A

Electrochemistry. Cyclic voltammetry (CV) was performed in a 3-electrode cell under an argon atmosphere with a glassy carbon working electrode (A = 0.031 cm^2), platinum counter electrode, and $Ag/AgNO_3$ (0.01 M, MeCN) reference electrode. Acetonitrile used for electrochemical measurements was purchased from Fisher (ACS grade), distilled over calcium hydride, and degassed with a dinitrogen purge before use. Ferrocene (Fc, 99%) used as an internal standard was purchased from Sigma and recrystallized from hexane. All potentials are reported vs. the $Fc^{0/+}$ redox couple. Bulk electrolysis studies were performed in a two-compartment cell separated by a glass frit. The working and counter electrodes were carbon felt, and the reference electrode was $Ag/AgNO_3$ (0.01 M, MeCN). Ferrocene was used in the counter electrode compartment as a sacrificial reductant. Working electrodes for all experiments were polished with alumina and diamond polish (1 μM), followed by electrochemical stripping in a 0.1 M $(TBA)PF_6$ acetonitrile solution (500 scans, 1 V/s, 0 to -2 V vs. $Fc^{0/+}$).

Overpotential Determination. Overpotential was determined by the exact method used by Ott and coworkers,[37] and is given relative to the corresponding $E^{Pt}_{1/2}$ obtained on a freshly polished Pt electrode under exactly the same conditions. The data reported in ref. 1 are directly relevant to the complexes reported here since our electrochemical experiments utilized the same solvent and acids (in nearly identical concentration ranges), as well as overall similar catalysts. Specifically, since all catalysts reported here reach activity saturation within roughly 100 equivalents of acetic acid, using 1 mM catalyst concentrations (i.e. acid concentrations do not exceed 0.2 M), the half-wave potential (E_{cat}) observed for platinum at [AcOH] of 0.2 M by Ott and coworkers, -1.48 V vs. $Fc^{0/+}$, was used to calibrate overpotentials for all catalysts reported here.

Gas Chromatography. Gas chromatography (GC) experiments in combination with bulk electrolysis studies for the measurement of dihydrogen gas were performed with a SRI 8610C

View Article Online
DOI: 10.1039/C5DT03744A

gas chromatograph equipped with a thermal conductivity detector (TCD) and a flame ionization detector (FID), as well as MS13X (6') and Hayesep-D (6') columns using dinitrogen (99.999% pure) as the electrochemical cell carrier gas with a flow rate of 3 mL/min. For the bulk electrolysis experiments, injections into the detector were made every ten minutes and dihydrogen evolution volumes were quantified for these times. To calculate the amount of hydrogen produced between the 10 minutes intervals, the rate of hydrogen produced per minute at the two intervals was averaged (($R_{x\ min}$ + $R_{x+10\ min}$))/2), and this average rate was used for an estimate of the produced H_2 volume over the ten minute interval ($V_{interval}$ = $R_{x-(x+10)\ avg}$ (V/min) * 10 min). Cumulative volumes were obtained by taking the sum of the aforementioned volumes from each time span. Faradaic efficiency was calculated as the molar sum of the evolved dihydrogen divided by half of the total electron charge passed in the same time frame.

X-Ray Crystallography. All structural data was collected on a Rigaku AFC10K Saturn 944+ CCD-based X-ray diffractometer equipped with a low temperature device and a Micromax-007HF Cu-target micro-focus rotating anode (λ = 1.54187 Å) operated at 1.2 kW power (40 kV, 30 mA). The X-ray intensities were measured at 85(1) K with the detector placed at a distance of 42.00 mm from the crystal. Analysis of the data showed negligible decay during data collection; the data were processed with CrystalClear 2.0 and corrected for absorption. The structures were solved and refined with the Bruker SHELXTL (version 2008/4) software package. Details about the structure determinations are provided in the Supporting Information.

Computational Methods. All geometry optimizations and frequency calculations were performed with the Gaussian 09 program package[52] with the BP86 functional and the TZVP basis set (as implemented in Gaussian 09).

View Article Online
DOI: 10.1039/C5DT03744A

General Preparation of diphosphine amine ligands:

Our method is a modification of a similar diphosphine synthesis reported by Imhoff et. al:[53] Chlorodiphenylphopshine (1.08 mL, 2 mmol) was added dropwise to a stirring solution of the selected primary amine (1 mmol) and triethylamine (1.4 mL, 10 mmol) in methylene chloride, causing a fine white precipitate to form. The mixture was allowed to stir overnight, after which time solvent was removed in vacuo. The solids were thoroughly washed with methanol (5x, 20 mL) and the filtered white product was dried by vacuum. The product was recrystallized from a dichloromethane/hexane solution at room temperature.

$(C_6H_5)_2PN(^iPr)P(C_6H_5)_2$

Recrystallization afforded the product as a white solid with a yield of 89%. ^{1}H-NMR (400 MHz, $CDCl_3$): δ_H = 7.23-7.42 (m, 20H, $(P(C_6H_5)_2)_2$), 3.2 (m, 1H, ^{i}Pr), 0.63 (d, 6H, ^{i}Pr) ppm. $^{31}P\{^1H\}$-NMR (202 MHz, $CDCl_3$): δ_P = 40 ppm (broad).

$(C_6H_5)_2PN(C_6H_5)P(C_6H_5)_2$

Recrystallization afforded the product as a white solid with a yield of 85%. ^{1}H-NMR (400 MHz, CD_2Cl_2): δ_H = 7.23-7.4 (m, 20H, $(P(C_6H_5)_2)_2$), 6.94 (m, 3H, NC_6H_5), 6.64 (d, 2H, NC_6H_5) ppm. $^{31}P\{^1H\}$-NMR (202 MHz, CD_2Cl_2): δ_P = 68.5 ppm.

$(C_6H_5)_2PN(p\text{-}C_6H_4Br)P(C_6H_5)_2$

Recrystallization afforded the product as a white solid with a yield of 80%. ^{1}H-NMR (500 MHz, CD_2Cl_2): δ_H = 7.2-7.55 (m, 20H, $(P(C_6H_5)_2)_2$), 6.74 (d, 2H, NC_6H_4Br), 6.5 (d, 2H, NC_6H_4Br) ppm. $^{31}P\{^1H\}$-NMR (202 MHz, CD_2Cl_2): δ_P = 69.2 ppm.

$(C_6H_5)_2PN(p\text{-}C_6H_4F)P(C_6H_5)_2$

Recrystallization afforded the product as a white solid with a yield of 87%.^{1}H-NMR (500 MHz, CD_2Cl_2): δ_H = 7.26-7.53 (m, 20H, $(P(C_6H_5)_2)_2$), 6.58 (m, 2H, NC_6H_4F) 6.45 (m, 2H, NC_6H_4F) ppm. $^{31}P\{^1H\}$-NMR (202 MHz, CD_2Cl_2): δ_P = 70.3 ppm. ^{19}F-NMR (348 MHz, CD_2Cl_2): δ_F = -117.4 ppm.

$(C_6H_5)_2PN(CH_2(p\text{-}C_6H_4F))P(C_6H_5)_2$

View Article Online
DOI: 10.1039/C5DT03744A

Recrystallization afforded the product as a white solid with a yield of 90%. ^{1}H-NMR (500 MHz, CD_2Cl_2): δ_H = 7.51-7.91 (m, 20H, $(P(C_6H_5)_2)_2$), 6.6 (m, 2H, $N(CH_2)C_6H_4F$), 6.4 (m, 2H, $N(CH_2)C_6H_4F$), 4.0 (m, 2H, $N(CH_2)C_6H_4F$) ppm. $^{31}P\{^{1}H\}$-NMR (202 MHz, CD_2Cl_2): δ_P = 72.5 ppm. ^{19}F- NMR (348 MHz, CD_2Cl_2): δ_F = -112.4 ppm.

$(C_6H_5)_2PN((CH_2)_4C_6H_5)P(C_6H_5)_2$

Recrystallization afforded the product as a colorless oil with a yield of 78%. ^{1}H-NMR (500 MHz, CD_2Cl_2): δ_H = 7.0-8.2 (m, 25H, $(P(C_6H_5)_2)_2$ and $N((CH_2)_4C_6H_5)$, 2.98 (m, 2H, $N((CH_2)_4C_6H_5)$, 2.6 (m, 2H, $N((CH_2)_4C_6H_5)$, 1.54 (m, 2H, $N((CH_2)_4C_6H_5)$, 1.13 (m, 2H, $N((CH_2)_4C_6H_5)$ ppm. $^{31}P\{^{1}H\}$-NMR (202 MHz, CD_2Cl_2): δ_P = 42.9 ppm.

$(C_6H_5)_2PN((CH_2)C_{14}H_9)P(C_6H_5)_2$

Recrystallization afforded the product as a white solid with a yield of 86%. ^{1}H NMR (400 MHz, CD_2Cl_2): δ_H = 7.47-8.75 (m, 9H, $N(CH_2)C_{14}H_9$), 7.2-7.4 (m, 20H, $(P(C_6H_5)_2)_2$), 5.1 (m, 2H, $(N(CH_2)C_{14}H_9)$) ppm. $^{31}P\{^{1}H\}$-NMR (202 MHz, CD_2Cl_2): δ_P = 58.9 ppm.

$(C_6H_5)_2PN(p\text{-}C_6H_4C{\equiv}CH)P(C_6H_5)_2$

Recrystallization afforded the product as a beige solid with a yield of 60%. ^{1}H-NMR (500 MHz, CD_2Cl_2): δ_H = 7.24-7.39 (m, 20H, $(P(C_6H_5)_2)_2$), 7.0 (d, 2H, $(p\text{-}HC{\equiv}CC_6H_4)$), 6.5 (d, 2H, $(p\text{-}HC{\equiv}CC_6H_4)$), 3.1 (s, 1H, $(p\text{-}HC{\equiv}CC_6H_4)$) ppm. $^{31}P\{^{1}H\}$-NMR (202 MHz, CD_2Cl_2): δ_P = 64.3 ppm.

$(C_6H_5)_2PN(3\text{-butyne})P(C_6H_5)_2$

Recrystallization afforded the product as a white solid with a yield of 76%. ^{1}H NMR (400 MHz, CD_2Cl_2): δ_H = 7.2-7.39 (m, 20H, $(P(C_6H_5)_2)_2$), 1.93 (m, 2H, $N((CH_2)_2C{\equiv}CH)$, 1.89 (s, 1H, $N((CH_2)_2C{\equiv}CH)$, 1.51 (m, 2H, $N((CH_2)_2C{\equiv}CH)$ ppm. $^{31}P\{^{1}H\}$ NMR (170 MHz, CD_2Cl_2): δ_P = 42.9 ppm.

General preparation of penta-coordinate iron and cobalt complexes:

Metal compounds were prepared following a procedure initially reported by Takács et al. (see Scheme 1 above):[54] In a large vial, 1,2-benzenedithiol (0.14 g, 1 mmol) and sodium methoxide (0.11 g, 2 mmol) were dissolved in 10 mL of methanol. In a Schlenk flask the selected diphosphine ligand (1 mmol) and ferrous sulfate heptahydrate (0.280 g, 1 mmol) were combined

View Article Online
DOI: 10.1039/C5DT03744A

in methanol (30 mL). The Schlenk flask was charged with 1 atm CO pressure, and the benzenedithiol solution was added dropwise via addition funnel to the mixture while stirring. Addition of this solution caused an immediate change in color from light yellow to reddish-brown. The mixture was allowed to stir under CO pressure for 5 hours, after which time the solvent was removed in vacuo. The resulting solid was washed with methylene chloride and filtered, the filtrate being collected and reduced in vacuo to a dark red-black solid. Flash column chromatography of the crude product over neutral silica gel in a 1:1 dichloromethane/hexane solvent mixture yielded complexes determined to be pure by ^{31}P and ^{1}H NMR in most cases (exceptions are noted below).

[Fe($S_2C_6H_4$)((C_6H_5)$_2$PN(^{i}Pr)P(C_6H_5)$_2$)CO] (1)

Column chromatography of the product afforded a reddish-brown solid of **1** in 60% yield. Single crystals suitable for X-ray diffraction were obtained by recrystallization in CH_2Cl_2/hexane layered solutions with slow evaporation at -32ºC. EA calc (x0.75 CH_2Cl_2): C 58.35, H 4.55, N 1.95; found: C 59.42, H 4.77, N 2.09. ^{1}H-NMR (400 MHz, $CDCl_3$): δ_H = 7.13-8.2 (m, 24H, (P(C_6H_5)$_2$)$_2$) and $S_2C_6H_4$), 3.47 (m, 1H, ^{i}Pr), 0.62 (d, 6H, ^{i}Pr) ppm. ^{31}P{^{1}H}-NMR (202 MHz, $CDCl_3$): δ = 105.4 ppm; IR (KBr): ν_{max}/cm^{-1} 1932 ν(C-O). APSI mass spectrum (positive mode): *m/z* = 623.9 (M – CO + H)$^+$.

[Fe($S_2C_6H_4$)((C_6H_5)$_2$PN(C_6H_5)P(C_6H_5)$_2$)CO] (2)

Column chromatography of the product afforded a reddish-brown solid of **2** in 65% yield. Recrystallization of this product in CH_2Cl_2/hexane layered solutions was required to remove residual impurities and provide pure compound. EA calc: C 64.82, H 4.26, N 2.04; found: C 64.25, H 5.05, N 1.93. ^{1}H-NMR (400 MHz, CD_2Cl_2): δ_H = 7.05-8.16 (m, 24H, (P(C_6H_5)$_2$)$_2$) and $S_2C_6H_4$), 7 (m, 2H, N(C_6H_5)), 6.6 (m, 2H, N(C_6H_5)) ppm. ^{31}P{^{1}H}-NMR (170 MHz, CD_2Cl_2): δ_P = 112.7 ppm. IR (KBr): ν_{max}/cm^{-1} 1935 ν(C-O).

[Fe($S_2C_6H_4$)((C_6H_5)$_2$PN(*p*-C_6H_4Br)P(C_6H_5)$_2$)CO] (3)

Column chromatography of the product afforded a reddish-brown solid of **3** in 40% yield. Recrystallization of this product in CH_2Cl_2/hexane layered solutions was required to remove residual impurities and provide pure compound. ^{1}H-NMR (500 MHz, CD_2Cl_2): δ_H = 7.15-8.18 (m, 24H, (P(C_6H_5)$_2$)$_2$) and $S_2C_6H_4$), 7.1 (m, 2H, N(*p*-BrC_6H_5)), 6.4 (m, 2H, N(*p*-BrC_6H_5)) ppm. ^{31}P{^{1}H}-NMR (202 MHz, CD_2Cl_2): δ_P = 113.5 ppm. IR (KBr): ν_{max}/cm^{-1} 1934 ν(C-O).

View Article Online
DOI: 10.1039/C5DT03744A

[Fe($S_2C_6H_4$)((C_6H_5)$_2$PN(p-C_6H_4F)P(C_6H_5)$_2$)CO] (4)

Column chromatography of the product afforded a reddish-brown solid of **4** in 60% yield. EA calc: C 63.17, H 4.01, N 1.99; found: C 62.19, H 4.22, N 1.95. ^{1}H-NMR (500 MHz, CD_2Cl_2): δ_H = 7.1-8.2 (m, 24H, (P(C_6H_5)$_2$)$_2$) and $S_2C_6H_4$), 6.74 (m, 2H, N(*p*-FC_6H_5)), 6.5 (m, 2H, N(*p*-FC_6H_5)) ppm. ^{31}P{^{1}H}-NMR (202 MHz, CD_2Cl_2): δ_P = 113.5 ppm. ^{19}F- NMR (348 MHz, CD_2Cl_2): δ_F = -114.2 ppm. IR (KBr): ν_{max}/cm^{-1} 1935 ν(C-O).

[Fe($S_2C_6H_4$)((C_6H_5)$_2$PN(CH_2(p-C_6H_4F))P(C_6H_5)$_2$)CO] (5)

Column chromatography of the product afforded a reddish-brown solid of **5** in 55% yield. Single crystals suitable for X-ray diffraction were obtained by recrystallization in CH_2Cl_2/hexane layered solutions with slow evaporation at -32ºC. EA calc: C 63.61, H 4.21, N 1.95; found: C 63.19, H 4.18, N 1.97. ^{1}H-NMR (500 MHz, CD_2Cl_2): δ_H = 7.13-8.55 (m, 24H, (P(C_6H_5)$_2$)$_2$) and $S_2C_6H_4$), 6.55 (m, 2, N(CH_2)C_6H_4F), 6.45 (m, 2, N(CH_2)C_6H_4F), 4.5 (m, 2, N(CH_2)C_6H_4F); ^{31}P{^{1}H}-NMR (202 MHz, CD_2Cl_2): δ_P = 111.4 ppm. ^{19}F-NMR (348 MHz, CD_2Cl_2): δ_F = -115.1 ppm. IR (KBr): ν_{max}/cm^{-1} 1931 ν(C-O).

[Fe($S_2C_6H_4$)((C_6H_5)$_2$PN((CH_2)$_4C_6H_5$)P(C_6H_5)$_2$)CO] (6)

Column chromatography of the product afforded a reddish-brown solid of **6** in 67% yield.^{1}H-NMR (500 MHz, CD_2Cl_2): δ_H = 7.1-8.1 (m, 27H, (P(C_6H_5)$_2$)$_2$), N((CH_2)$_4C_6H_5$) and $S_2C_6H_4$), 6.88 (d, 2H, N((CH_2)$_4C_6H_5$)), 2.94 (m, 2H, N((CH_2)$_4C_6H_5$)), 2.3 (d, 2H, N((CH_2)$_4C_6H_5$)), 2.15 (d, 2H, N((CH_2)$_4C_6H_5$)), 1.19 (d, 2H, N((CH_2)$_4C_6H_5$)) ppm. ^{31}P{^{1}H}-NMR (202 MHz, $CDCl_3$): δ_P = 109.4 ppm. IR (KBr): ν_{max}/cm^{-1} 1932 ν(C-O).

[Fe($S_2C_6H_4$)((C_6H_5)$_2$PN($CH_2C_{14}H_{10}$)P(C_6H_5)$_2$)CO] (7)

Column chromatography of the product afforded a reddish-brown solid of **7** in 63% yield. ^{1}H-NMR (400 MHz, CD_2Cl_2): δ_H = 6.8-8.2 (m, 33H, N(CH_2)$C_{14}H_9$), (P(C_6H_5)$_2$)$_2$) and $S_2C_6H_4$), 5.3 (m, 2H, N(CH_2)$C_{14}H_9$) ppm. ^{31}P{^{1}H}-NMR (202 MHz, CD_2Cl_2): δ_P = 110.8 ppm. IR (KBr): ν_{max}/cm^{-1} 1931 ν(C-O).

[Fe($S_2C_6H_4$)((C_6H_5)$_2$PN(p-$C_6H_4C{\equiv}CH$)P(C_6H_5)$_2$)CO] (8)

Column chromatography of the product afforded a reddish-brown solid of **8** in 66% yield. ^{1}H-NMR (500 MHz, CD_2Cl_2): δ_H = 7.0-8.2 (m, 24H, (P(C_6H_5)$_2$)$_2$) and $S_2C_6H_4$), 6.9 (d, 2H, N(p-$HC{\equiv}CC_6H_4$), 6.4 (d, 2H, N(p-$HC{\equiv}CC_6H_4$), 3.2 (d, 1H, N(p-$HC{\equiv}CC_6H_4$) ppm. ^{31}P{^{1}H}-NMR (202 MHz, CD_2Cl_2): δ_P = 113.4 ppm. IR (KBr): ν_{max}/cm^{-1} 1939 ν(C-O).

[Fe($S_2C_6H_4$)((C_6H_5)$_2$PN((CH_2)$_2C{\equiv}CH$)P(C_6H_5)$_2$)CO] (9)

Column chromatography of the product afforded a reddish-brown solid of **9** in 45% yield. ^{1}H-NMR (400 MHz, $CDCl_3$): δ_H = 7.12-8.1 (m, 24H, (P(C_6H_5)$_2$)$_2$) and $S_2C_6H_4$), 1.93 (m, 2H,

View Article Online
DOI: 10.1039/C5DT03744A

$N((CH_2)_2C{\equiv}CH)$, 1.89 (s, 1H, $N((CH_2)_2C{\equiv}CH)$, 1.51 (m, 2H, $N((CH_2)_2C{\equiv}CH)$ ppm. $^{31}P\{^1H\}$-NMR (202 MHz, CD_2Cl_2): δ_P = 109.2 ppm; IR (KBr): ν_{max}/cm^{-1} 1927 ν(C-O).

[Co($S_2C_6H_4$)((C_6H_5)$_2$PN(^{i}Pr)P(C_6H_5)$_2$)CO] (10)

A reddish-brown solid with high luster was collected with a crude yield of 70%. Single reddish-brown crystals confirmed as pure product and suitable for X-ray diffraction were obtained by recrystallization in CH_2Cl_2/hexane layered solution with slow evaporation at room temperature. $^{31}P\{^1H\}$ NMR (202 MHz, CD_2Cl_2): δ_P = 80.9 ppm; IR (KBr): ν_{max}/cm^{-1} 1988 ν(C-O). APSI mass spectrum (positive mode): *m/z* = 627.0 $(M - CO + H)^+$.

Results

1. Characterization

In all cases, dropwise addition of the deprotonated dithiolate ligand in methanol to a suspension of ferrous sulfate and the respective PNP diphosphines in methanol under a carbon monoxide atmosphere led to a distinct color change of the solution to deep reddish-brown. Removal of solvent after 5 hours and subsequent extraction of the products into methylene chloride provided the corresponding iron species in crude yields of 60-90%.[54] Flash chromatography over neutral silica generally gave the compounds in high purity as assessed by ^1H, ^{31}P and ^{19}F NMR (**Figures S1-3**), infrared spectroscopy (IR) (**Figure S4**), and mass spectrometry (MS). IR spectra of the iron complexes consistently show a single ν(C-O) stretch at frequencies of 1927-1939 cm^{-1}, indicative of species containing a single carbonyl ligand. Two intense bands are also present at energies of 1434 and 694 cm^{-1} that are characteristic of the phenyl groups of the diphosphine ligand, and that vary by a minimal amount (~1-2 cm^{-1}) with

View Article Online
DOI: 10.1039/C5DT03744A

Table 1. Penta-coordinate iron compounds prepared here and selected properties

R= 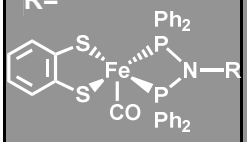	#	$\nu(C\text{-}O)_{max}$ (cm^{-1})	^{31}P NMR δ_P (ppm)	^{19}F NMR δ_F (ppm)	$E_{1/2}$ (V) *	η (V) ◊	i_{cat}/i_p	TOF (s^{-1}) †	k_{cat} ($M^{-1}\ s^{-1}$) ‡
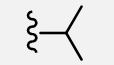	**1**	1932	105.4	N/A	-1.69	0.21	2.7	1.38	120
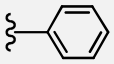	**2**	1935	112.7	N/A	-1.62	0.14	2.9	1.58	235
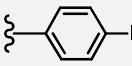	**3**	1934	113.5	N/A	-1.57	0.09	2.26	0.96	144
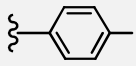	**4**	1935	113.5	-120	-1.61	0.13	2.61	1.28	301
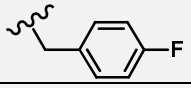	**5**	1931	111.4	-115	-1.66	0.18	4.28	3.46	1243
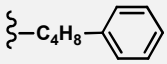	**6**	1932	109.4	N/A	-1.63	0.15	4.32	3.51	1375
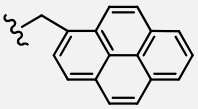	**7**	1931	110.8	N/A	-1.68	0.20	2.45	1.13	197
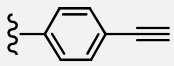	**8**	1939	113.4	N/A	-1.6	0.12	1.22	0.28	8
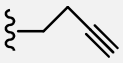	**9**	1927	109.2	N/A	-1.63	0.15	2.61	1.28	109

* Potentials are reported versus a ferrocene/ferrocenium internal standard (0.64 V vs. NHE)
◊ Overpotentials reported are lower-end estimates vs. Pt with 0.1 M acetic acid in acetonitrile.
† Turnover frequencies were calculated using **equation 1** at the $E_{1/2}$ potential for the corresponding complex with an [AcOH] of 0.1 M and a catalyst concentration of 1 mM.
‡ Bimolecular rate constants calculated from the slope of the i_{cat} vs. $[ACOH]^{1/2}$ plot.

substitution at the amine position. The ^{31}P NMR spectra of the iron complexes show a single sharp resonance at 105-113 ppm depending on the substituents at the PNP amine group (**Table 1).** The molecular structures of **1** and **5** have been confirmed by X-ray crystallography, showing penta-coordinate complexes with distorted square-pyramidal geometries and an axial carbonyl ligand (**Figure 1**). The Fe-P and Fe-S bond lengths observed for **1** and **5** are nearly identical to the 'PCNCP' ligated iron complex, $[Fe(S_2C_6H_4)((C_6H_5)_2PCH_2N(dep)CH_2P(C_6H_5)_2)(CO)]$, reported by Ott and coworkers, as well as to the $P(FeCp_2)P$ ligated iron complex, $[Fe(S_2C_6H_4)((C_6H_5)_2P(FeCp_2)\ P(C_6H_5)_2)(CO)]$, reported by Jones and coworkers (**Table 2**).[28,37]

View Article Online
DOI: 10.1039/C5DT03744A

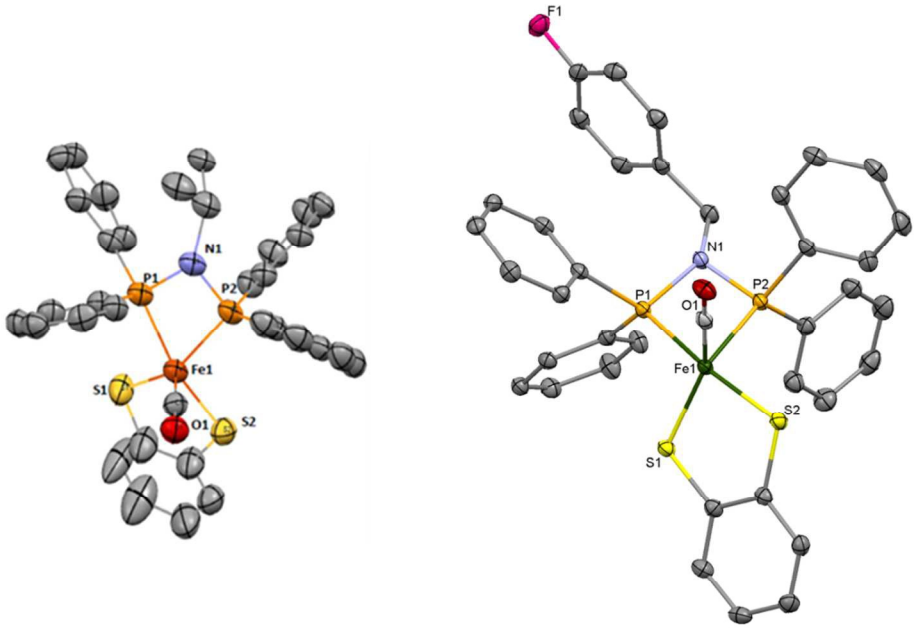

Figure 1. Crystal structures of $[Fe(S_2C_6H_4)((C_6H_5)_2PN(^iPr)P(C_6H_5)_2)(CO)]$ (**1**) (*left*) and $[Fe(S_2C_6H_4)((C_6H_5)_2PN(p\text{-fluorobenzyl})P(C_6H_5)_2)(CO)]$ (**5**) (*right*) with ellipsoids shown at 50% probability. Hydrogen atoms are omitted for clarity. Selected bond distances [Å] and angles [degrees]: (**1**) Fe1-P1 2.203(15), Fe1-P2 2.2(13), Fe1-S1 2.161(13), Fe1-S2 2.189(14), P1-N1 1.71(4), P2-N1 1.703(4), P1---P2 2.577(17), S1---S2 3.082, S1-Fe1-S2 90.25(5), P1-Fe1-P2 71.65(5), Fe-P-N-P torsion 6.74. (**5**) Fe1-P1 2.215(6), Fe1-P2 2.144(6), Fe1-S1 2.166(6), Fe1-S2 2.21(6), P1-N1 1.718(16), P2-N1 1.708(17), P1---P2 2.583(7), S1---S2 3.096, S1-Fe1-S2 90.03(2), P1-Fe1-P2 72.65(2), Fe-P-N-P torsion 8.19.

The S-Fe-S bond angles also show strong similarities across these compounds, as expected for the identical dithiolate ligand. In contrast, the P-Fe-P bond angle is significantly larger (by over 15º) in the complex reported by Jones, and even more so (over 17º) in Ott's compound. Most notably, the torsion angles of the Fe-P-N-P ring in the complexes reported here are very small (< 9º), showing a nearly planar ring structure. In comparison, the Fe-P-N-P unit of Ott's complex has a torsion angle of 14º, and shows a distinctly non-planar chair conformation for the whole Fe-P-C-N-C-P unit (**Figure S6**). Jones' compound exhibits a similarly large torsion angle of 18º for its Fe-P-Fe-P unit. These differences highlight the more rigid, conjugated structure of the FePNP ring in the complexes reported here. Comparison of C-O stretching frequencies shows strong similarity for **1** and **5** ($\nu(C\text{-}O)_{MeCN}$ = 1933 and 1931 cm^{-1}, respectively) compared to the compound reported by Ott and coworkers ($\nu(C\text{-}O)_{MeCN}$ = 1932 cm^{-1}), while both sets of

View Article Online
DOI: 10.1039/C5DT03744A

Table 2. Comparison of selected bond lengths [Å] and angles [º] for selected penta-coordinate iron compounds.

Complex (#)	M-S1	M-S2	M-P1	M-P2	P-M-P	S-M-S	MPNP torsion	τ (0-1)
1	2.161(13)	2.189(14)	2.203(15)	2.2(13)	71.65(5)	90.25(5)	6.74	0.26
5	2.166(6)	2.21(6)	2.215(6)	2.144(6)	72.65(2)	90.03(2)	8.19	0.73
10	2.194(9)	2.202(8)	2.188(9)	2.187(8)	72.13(3)	91.16(3)	3.77	0.03
$Fe(S_2C_6H_4)((C_6H_5)_2PCH_2N(dep)CH_2P(C_6H_5)_2)(CO)$ [1*]	2.187	2.187	2.208	2.212	89.59	89.32	14.01	0.13
$Fe(S_2C_6H_4)((C_6H_5)_2P(CH_2N^{Ph}CH_2)_2P(C_6H_5)_2)(CO)$ [41*]	2.21	2.17	2.14	2.17	80.5	88.7	29/58	0.22
$Fe(S_2C_6H_4)((C_6H_5)_2P(FeCp_2)P(C_6H_5)_2)(CO)$ [30*]	2.2	2.177	2.222	2.225	87.49	89.31	18.2 (FePFeP)	0.72

*dep: 1,1-diethoxypropane; $FeCp_2$: bis(cyclopentadienyl)iron or ferrocene; N^{Ph}: $N(C_6H_5)$.

compounds show a somewhat higher ν(C-O) than that reported by Jones and coworkers ($\nu(C\text{-}O)_{DCM}$ = 1915 cm^{-1}). Addison's tau (τ) values (defined as $\tau = (\beta - \alpha)/60$)[55] were determined for the penta-coordinate iron complexes as a measure of distortion from an ideal square-pyramidal geometry (τ = 0) or an ideal trigonal-bipyramidal geometry (τ = 1) with S1-Fe1-P2 constituting α and S2-Fe1-P1 constituting β for $\tau = (\beta - \alpha)/60$. Tau values for compounds **1** and **5** are 0.26 and 0.73 respectively, showing a substantial change in solid state geometry despite a minimal change in the overall PNP structure. While the compounds reported by Ott and coworkers have a square-pyramidal structure more closely related to **1**, the ferrocene derivatives reported by Jones and coworkers are observed to have a nearly identical tau value to **5**.

Cyclic voltammograms of the penta-coordinate iron compounds in acetonitrile solution show reversible redox waves, assigned to the $Fe^{II/I}$ couple, at potentials ranging from -1.57 to -1.69 V versus $Fc^{0/+}$ (**Figure 2**). All compounds are observed to have i_{pa}/i_{pc} separations of approximately

View Article Online
DOI: 10.1039/C5DT03744A

0.07 V, as is observed for the ferrocene internal standard under identical conditions. For most compounds, the i_{pa}/i_{pc} ratio consistently gave values of 1 (±0.1) at all scan rates, suggesting chemical reversibility with no decomposition occurring after reduction on the voltammogram time scale (**Figure S11**). Complexes **2** and **8** have disproportionately smaller anodic peaks compared to cathodic peaks ($i_{pa}/i_{pc} < 0.9$). For several of the compounds, a small decrease in the i_{pa}/i_{pc} ratio with increasing scan rates is observed, most noticeably for **2** and **8**. As it is more significant at higher scan rates, this decrease in i_{pa}/i_{pc} is likely due to a somewhat slow geometric reorganization step for these compounds (see DFT results below), resulting in a mixture of conformations with slightly offset oxidation potentials and a slightly lower i_a overall at higher scan rates. With the exceptions of these complexes, all i_c and i_a values are seen to increase proportionally to [scan rate]$^{1/2}$ (**Figure S11**), and no significant change in peak potentials (E_{pa} and E_{pc}) is observed upon varying the scan rate.

2. Electrocatalytic Studies

View Article Online
DOI: 10.1039/C5DT03744A

Upon addition of acetic acid (pKa_{MeCN} = 22.3), the cathodic waves of the iron species increased approximately linearly with acid concentration, which simultaneously occurred with the subsiding of the corresponding anodic waves. This behavior is indicative of electrocatalytic proton reduction from acetic acid, and consistently gave half-maximum wave potential (E_{cat}) values that directly coincide with the $E_{1/2}$ of each iron species. Background reduction of acetic acid protons by glassy carbon at these potentials and acid concentrations is negligible as shown in **Figure 2**. Importantly, activity occurs at potentials that correspond to only very slight overpotentials for proton reduction, as compared to the same process (acetic acid reduction, 0.1M) by platinum under identical conditions (see Experimental Section).[37] A half-wave potential (E_{cat}) of only -1.57 V vs. $Fc^{0/+}$ is displayed by the compound with the 4-bromophenyl substituent at the PNP amine (**3**), corresponding to an overpotential of only 0.09 V vs. platinum, the lowest for all of the compounds reported here. Discussion of overpotential with respect to the thermodynamically reversible reduction of acetic acid is provided in the SI, Section 5. The

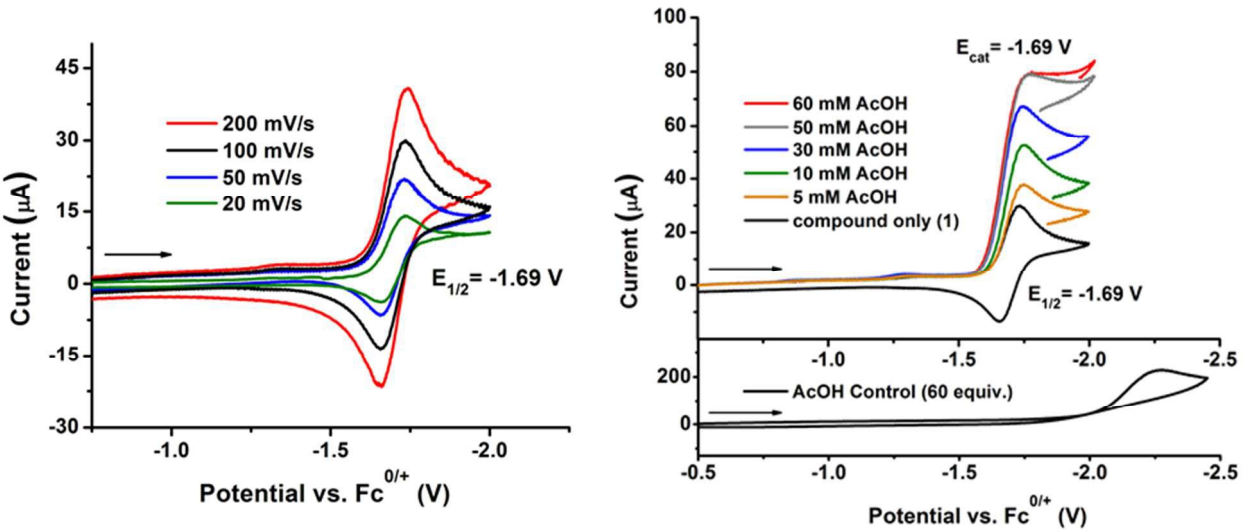

Figure 2. *Left:* Cyclic voltammetry of a 2mM solution of **1** in acetonitrile at various scan rates *Right:* Cyclic voltammetry of **1** at a scan rate of 100 mV/s with the addition of increasing equivalents of acetic acid. Solutions were 0.1 M $(TBA)PF_6$ and ferrocene was used as an internal standard. The working electrode was a glassy carbon disc, the reference was a non-aqueous $Ag/AgNO_3$ (0.01M) electrode, and the auxiliary electrode was a platinum disc.

View Article Online
DOI: 10.1039/C5DT03744A

overpotentials of all compounds are listed in Table 1. It is worth noting that the current increase for **8** is significantly lower than that for all other compounds, low enough that **8** could be considered inactive for proton reduction (within error).

The catalytic current increases linearly with catalyst concentration over the investigated range of catalysts [1.0-1.75 mM] at acid saturation conditions, indicative of a first order dependence of the rate on catalyst concentration (**Figure S10**). With lower acid concentrations, total catalysis is observed, where activity is limited only by diffusion of substrate (acid) to the electrode and catalytic activity increases linearly with acid concentration.[56] At higher acid concentrations (exact number of equivalents is dependent on the ligand substitution), catalytic plateau currents are approximately linear with $[AcOH]^{1/2}$ (**Figure S9**) until activity saturation behavior is observed. Bimolecular rate constants are calculated from the slopes of these plots with **equation 1** analogous to the methods used by Ott and coworkers to provide a direct comparison to their similar catalyst systems:

(1) $$\boldsymbol{I_p = FAC^0_{cat}\sqrt{D}\sqrt{2kC^0_S}}$$

Here, D is the diffusion coefficient as determined by the Randles Sevcik equation (**Equation S3**) to be 1 x 10^5 (+/- 0.2) cm^2/s, and A is the electrode area (0.031 cm^2). Rate constants from Equation 1 give a range of activities from 8 to 1375 M^{-1} s^{-1} (**Table 1**).[37] At the activity saturation point where the peak catalytic current (i_{cat}) is seen to be independent of acid concentration, rate estimates for each species can also be obtained from the ratio of the peak catalytic current to the cathodic current in the absence of acid (**equation 2**).[57]

(2) $$\boldsymbol{\frac{i_{cat}}{i_p} = \frac{2}{0.446}\sqrt{\frac{RTk_{obs}}{Fv}}}$$

Here, F = Faraday's constant and ν = scan rate (V/s). This method is used to calculate TOF for

View Article Online
DOI: 10.1039/C5DT03744A

the penta-coordinate species, varying from 0.28 to 3.51 s^{-1}, depending on the ligand substitution pattern as listed in **Table 1** (see Table for TOF measurement conditions).

Bulk electrolysis coupled with gas chromatography (GC) was used to monitor electrocatalytic dihydrogen production by **5** (1 mM) in acetonitrile solution from 0.04 M acetic acid (**Figure 3**). GC confirmed continued catalytic activity for 2 hours to produce a total of 87 micromoles of dihydrogen with 73% Faradaic efficiency. From this electrolysis data a turnover number (TON) of 6 has been calculated for **5**. After initial activity subsided (t = 2 hours), a second aliquot of acid was added; however, no significant resurgence in dihydrogen production was observed beyond control levels, confirming the compound's activity had not ceased due to acid depletion. Significant bleaching of the solution had occurred within the initial 2 hours of electrolysis. Solution IR analysis of the electrolysis solution at this time showed negligible signal intensity at the carbonyl ligand stretching frequency for **5** (1931 cm^{-1}), indicating the complex had degraded including loss of CO. ^{31}P NMR confirmed the degradation of **5** with complete loss of the

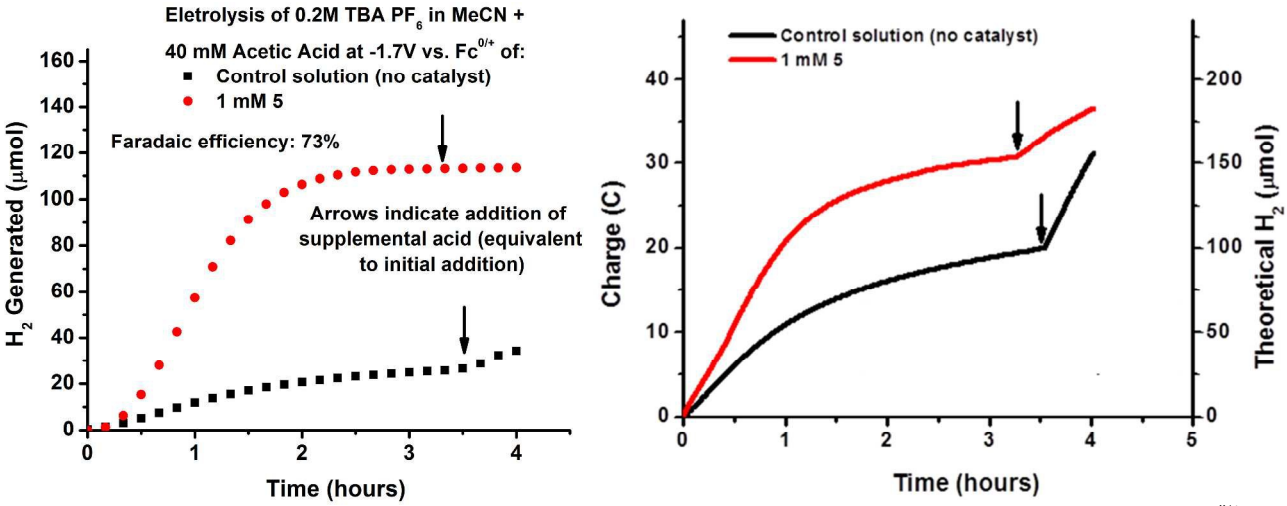

Figure 3. *Left:* Gas chromatography dihydrogen production measurement for bulk electrolysis at -1.7 V vs. $Fc^{0/+}$ of **5** (1 mM) with acetic acid (40 mM) in a 0.2 M $(TBA)PF_6$ acetonitrile solution. *Right:* Charge passed during the electrolysis experiment. 0.1 M $(TBA)PF_6$ and ferrocene was used as an internal standard. The working and auxiliary electrodes were carbon felt (4 cm^2), and the reference was a non-aqueous $Ag/AgNO_3$ (0.01M) electrode. Ferrocene (0.1 M) was used in the counter compartment as a sacrificial reductant. Arrows indicate addition of supplemental acid, equivalent to the initial addition.

View Article Online
DOI: 10.1039/C5DT03744A

resonance at 111.4 ppm, and decomposition was further evidenced by a change in solution color from reddish-brown to yellow.

The less than quantitative efficiency is likely due to trace amounts of ferrocenium hexafluorophosphate (the oxidized form of the sacrificial reductant) leaking through the glass frit and being reduced at the working electrode. This phenomenon is also observed in the control experiments, confirming that substantial non-faradaic charge is being passed in the absence of catalyst. Additional charge loss could be attributed to a possible reductive decomposition pathway for these catalyst species.

3. Mechanistic Studies

View Article Online
DOI: 10.1039/C5DT03744A

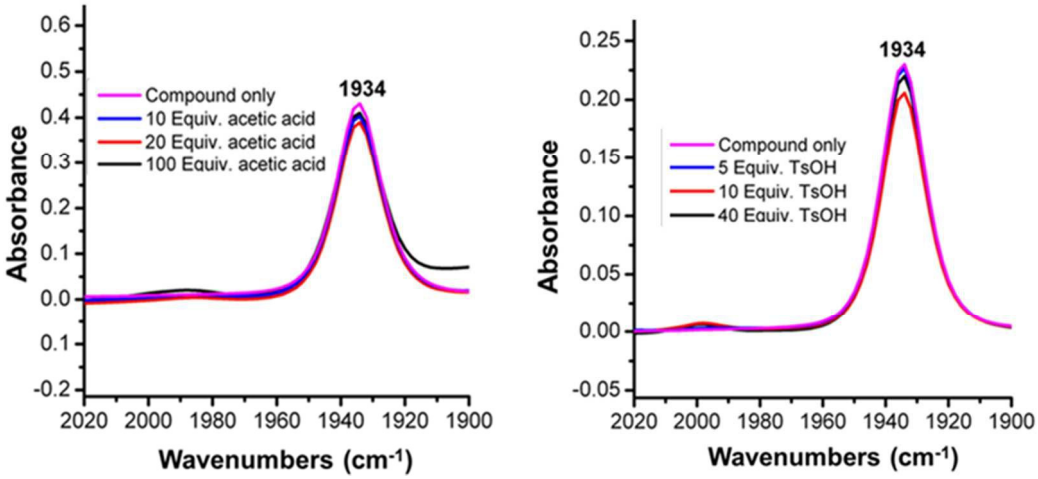

Figure 4. Variation of ν(C-O) for $[Fe(S_2C_6H_4)((C_6H_5)_2PN(^iPr)P(C_6H_5)_2)(CO)]$ (**1**) in acetonitrile solution upon the addition of acetic acid (*left*) and toluene sulfonic acid (*right*), monitored by solution IR spectroscopy.

Monitoring of the C-O stretching frequency of **1** in acetonitrile solution by IR spectroscopy upon the addition of acetic acid (pKa_{MeCN} = 22.3) shows no significant shift of the ν(C-O) band under these conditions (**Figure 4**). This result rules out chemical alteration of the catalyst by acetic acid prior to the reduction of the complexes, and is further supported by the fact that the catalytic onset potential for each iron complex with this acid is nearly identical to its $E_{1/2}$ value (Fe^{II}/Fe^{I} potential). These observations are consistent for all complexes investigated here (**1-9**) that differ in the PNP substitution pattern. The same results were obtained using the significantly stronger toluenesulfonic acid (TsOH, pKa_{MeCN} = 8.3). These results suggest that the Fe^{II} complexes cannot be protonated by the acids used for the electrocatalytic studies performed here, and that the initial mechanistic step for our penta-coordinate iron catalysts is a one-electron reduction. To observe intermediates after initial reduction, bulk electrolysis of species **1** was performed, and the reaction was monitored by solution IR spectroscopy (**Figure 5**). Upon applying a potential of -1.7 vs. $Fc^{+/0}$, a red shift in the carbonyl ligand stretching frequency of nearly 100 cm^{-1} was observed, showing a slightly broader and less intense signal at 1836 cm^{-1}.

View Article Online
DOI: 10.1039/C5DT03744A

This shift is indicative of the formation of a reduced Fe^{I}-CO species, and correlates well with the reduced $[Fe(S_2C_6H_4)((C_6H_5)_2P(CH_2N^{Ph}CH_2)_2P(C_6H_5)_2)(CO)]$ species observed by Ott and coworkers with a ν(C-O) band at 1850 cm^{-1}.[40] This species is assumed to be the reactive intermediate for hydride formation as no further reduction events are evident at this applied

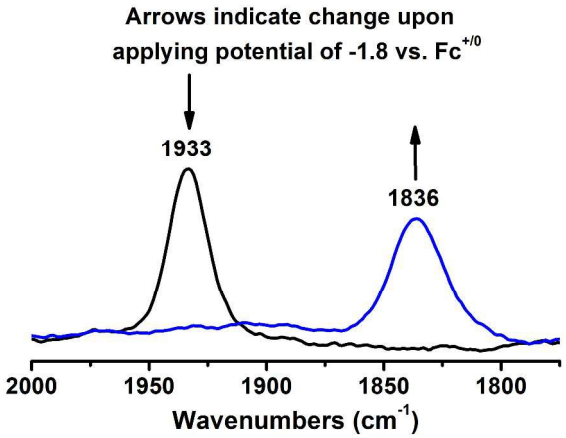

Figure 5. Bulk electrolysis at -1.8 V vs. $Fc^{+/0}$ of a 4 mM solution of **1** in acetonitrile with 0.1 M $(TBA)PF_6$ monitored by solution IR spectroscopy. The black trace is the spectrum of the compound prior to passing charge; the blue trace corresponds to the species formed during bulk electrolysis.

potential (no further carbonyl band shifting is observed with additional electrolysis time). Loss of the ν(C-O) signal at 1836 cm^{-1} for $\mathbf{1}^-$ was observed only several minutes after the applied potential was removed, and no substantial recovery of **1** as indicated by the ν(C-O) band at 1933 cm^{-1} was observed, suggesting decomposition by CO loss.

Density Functional Calculations

Given the similarity in overall structure for all $[Fe(S_2C_6H_4)(PNP)(CO)]$ derivatives reported here, full geometry optimizations of **1** (S = 0) with the BP86 functional and the TZVP basis set were performed as a representation of all the complexes investigated here. The optimized structure of **1** overall matched reasonably well with the crystal structure as shown in **Table 3**, with an average offset of 0.03 Å for iron-ligand bond lengths and 0.3 degrees for iron-ligand

View Article Online
DOI: 10.1039/C5DT03744A

bond angles. In contrast, both the FePNP torsion and τ values are somewhat underestimated, with a predicted torsion angle that is 4 degrees lower than that in the crystal structure and an estimated τ value of 0.01. Frequency calculations of **1** produce a single carbonyl stretch with ν(C-O) of 1951 cm^{-1}, fairly close to the experimental value of 1933 cm^{-1}.

Calculations on the reduced Fe^{I} species $\mathbf{1}^{-}$ (S = 1/2) show a relatively small change in bond lengths compared to **1**, with an increase of 0.06 and 0.08 Å for Fe-S1 and Fe-S2, respectively, and a decrease of only 0.02 Å for Fe-P1. The P1-Fe1-P2 bond angle has a similar change of approximately 2 degrees. Far more substantial changes in FePNP torsion angle and τ value are predicted upon reduction, with a 4 degree increase in torsion angle and an increase of τ from 0.01 to 0.7. This represents a substantial change in complex geometry upon reduction from an essentially ideal square pyramidal structure to a more closely trigonal bipyramidal geometry. Frequency calculations of $\mathbf{1}^{-}$ produce a single carbonyl stretch with ν(C-O) of 1886 cm^{-1}, substantially higher than the ν(C-O) value of 1836 cm^{-1} observed experimentally upon reduction of **1**.

Table 3. Select bond lengths [Å] and angles [º] for penta-coordinate iron species **1** as predicted by DFT calculations and comparison to crystal structure values. Calculations were performed with BP86/TZVP.

Structure source	Fe-S1	Fe-S2	Fe-P1	Fe-P2	P-Fe-P	S-Fe-S	FePNP torsion	τ (0-1)
Crystal structure of 1	2.16	2.189	2.203	2.2	72.66	90.03	6.74	0.26
DFT structure of 1	2.198	2.198	2.226	2.238	73.02	90.28	2.71	**0.01**
DFT structure of 1^{-}	2.255	2.286	2.206	2.24	72.93	88.38	6.26	**0.7**
DFT structure of 1^{-} - (CO)	2.216	2.226	2.152	2.164	73.35	91.06	0.01	0.19
DFT structure of 1^{-} (MeCN)	2.272	2.272	2.183	2.194	73.17	88.73	2.94	0.03

View Article Online
DOI: 10.1039/C5DT03744A

Loss of the ν(C-O) signal for **1**$^{-}$ after several minutes, as evidenced by IR spectroscopy, prompted DFT investigations of the reduced structure after the loss of CO (**1**$^{-}$ **- (CO)**, S = 1/2). The ΔE for CO loss from the low-spin Fe^{I} complex was calculated to be unfavorable by 45.6 kcal/mol, a substantial value for a process seen to be experimentally credible. While this value supports the slow timeframe of CO loss after reduction observed by IR spectroscopy, it likely also suggests an alternative chemical transformation prior to CO loss to promote this reaction and avoid such an energetically unfavorable pathway as direct loss from the reduced, five-coordinate complex.

Cobalt Analogs

View Article Online
DOI: 10.1039/C5DT03744A

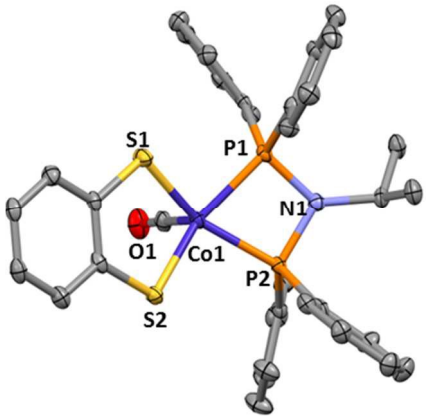

Figure 6. Crystal structure of [Co($S_2C_6H_4$)((C_6H_5)$_2$PN(^{i}Pr)P(C_6H_5)$_2$)(CO)] (**10**) with ellipsoids shown at 50% probability. Hydrogen atoms are omitted for clarity. Selected bond distances [Å] and angles [degrees]: Co1-P1 2.188(9), Co1-P2 2.187(8), Co1-S1 2.194(9), Co1-S2 2.202(8), P1-N1 1.695(2), P2-N1 1.708(2), P1---P2 2.576(10), S1---S2 3.140, S1-Co1-S2 91.16(3), P1-Co1-P2 72.13(3), Co-P-N-P torsion 3.77

The cobalt compound analogous to **1** was prepared following the same synthetic procedure as in the case of iron, but using a cobaltous sulfate reagent as the metal source. IR spectroscopic analysis of this compound (crude product) shows a single ν(C-O) band at 1988 cm^{-1} (**Figure S5**), suggesting the corresponding cobalt penta-coordinate compound had been formed with an analogous ligand environment as in the case of **1**. Mass spectrometry confirmed the presence of a species with *m/z* of 627, corresponding to the cobalt dithiolate diphosphine complex after the loss of the carbonyl ligand (as was seen by mass spectrometry analysis for the iron analog). Single crystals of **10** suitable for diffraction were afforded with some difficulty, and analysis confirmed the expected five-coordinate structure displaying a square pyramidal geometry with an axial carbonyl ligand, completely analogous to the iron complex (**Figure 6**).

Given the difficulty in obtaining pure product for **10**, electrochemical analysis was performed on the crude product. Cyclic voltammetry of this mixture showed a main redox feature at -1.57 V vs. $Fc^{0/+}$, while a minor feature attributed to an impurity was evident with an $E_{1/2}$ of -1.32 V (**Figure S8**). Upon the addition of tributylammonium hexafluorophosphate (Bu_3NH PF_6), an increasing cathodic current was observed at -1.63 V, corresponding to the $E_{1/2}$ of the more

View Article Online
DOI: 10.1039/C5DT03744A

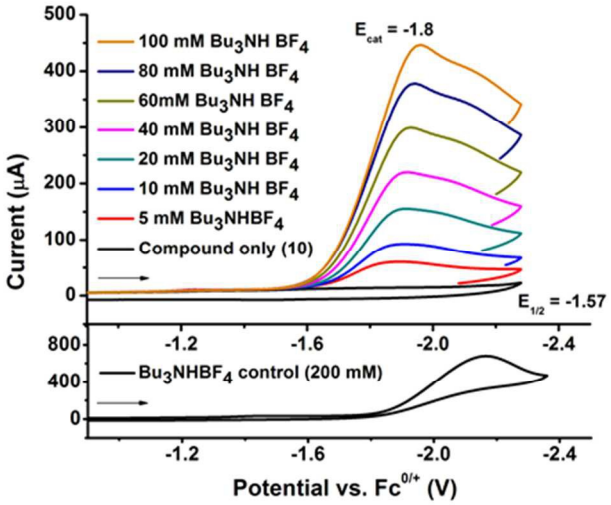

Figure 7. Cyclic voltammetry of **10** (2 mM) at a scan rate of 100 mV/s with the addition of increasing equivalents of $(Bu_3NH)BF_4$. Solutions contained 0.1 M $(TBA)PF_6$ as a supporting electrolyte and ferrocene was used as an internal standard. The working electrode was a glassy carbon disc, the reference was a non-aqueous $Ag/AgNO_3$ (0.01M) electrode, and the auxiliary electrode was a platinum disc electrode.

prominent redox feature in the CV of crude **10** (**Figure 7**). Increasing acid concentrations showed a linear increase in catalytic current; however, multiple features were apparent upon close analysis of the catalytic wave, suggesting the presence of multiple active species in the crude product or the availability of multiple mechanistic pathways at more negative potentials. A substantial cathodic shift of the E_{cat} was also evident with increasing acid concentration, indicating the species or mechanistic pathway giving rise to the more anodic portion of the wave was being altered with additional acid. Through rigorous chromatography and mechanistic studies (detailed in SI section 4), it was determined that the component of the crude product responsible for the sustained current response at high acid concentrations was not the penta-coordinate cobalt analog, but rather a cobalt bis(dithiolate) by-product similar to those reported independently by McNamara et al.[17]

Discussion

View Article Online
DOI: 10.1039/C5DT03744A

Scheme 2. Illustration of the delocalization of the nitrogen lone pair of the PNP ligand, leading to a planar FePNP ring.

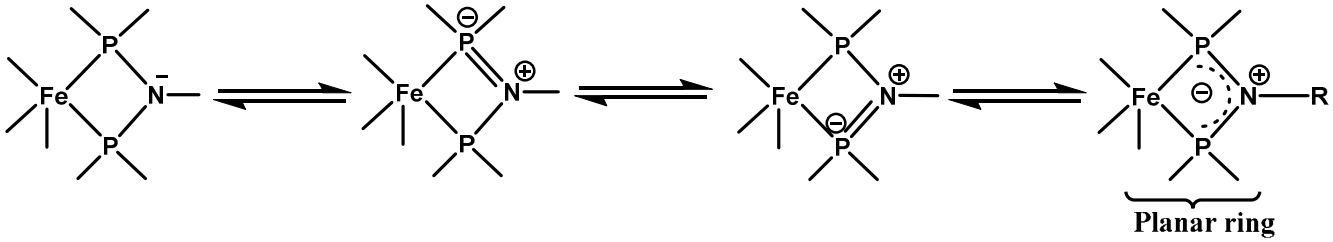

In this paper, we report a new series of five-coordinate Fe^{II}-CO complexes that serve as H_2 production catalysts with weak acids at very low overpotentials (relative to the thermodynamic activation potential for acetic acid). Our penta-coordinate iron compounds all contain a rigid $Fe(S_2C_6H_4)$(PNP) ligand structure and show very similar ν(C-O) frequencies, ^{31}P NMR resonances, and $E_{1/2}$ values. These results generally suggest that modification of the secondary ligand sphere of the PNP ligand has a limited effect on the geometrical structure and electron density at the metal center in the resulting complexes.

The penta-coordinate iron compound **1** exhibits a distorted square-pyramidal geometry with an Addison τ value (defined as $\tau = (\beta - \alpha)/60$)[55] of 0.26. The Fe-P-N-P- ring is nearly perfectly planar, confirming the rigid nature of the ligand moiety. This planar geometry around the nitrogen atom is surprising and is indicative of a conjugated ring structure (see **Scheme 2**). In comparison, the structures of the related complexes by Ott and coworkers, $[Fe(S_2C_6H_4)((C_6H_5)_2PCH_2N(dep)CH_2P(C_6H_5)_2)(CO)]$, and Jones and coworkers, $[Fe(S_2C_6H_4)((C_6H_5)_2P(FeCp_2)P(C_6H_5)_2)(CO)]$, show very similar core structures, but non-planar rings in the Fe-P-C-N-C-P and Fe-P-C-Fe-C-P units, respectively (**Figure S6**). As identical dithiolate and CO ligands are used in all three types of compounds, the reduced activity and lower overpotentials seen in the compounds reported here can be exclusively attributed to the structural differences from the 'PNP' diphosphine ligand used here.[28,37]

View Article Online
DOI: 10.1039/C5DT03744A

Electrochemical analysis of compounds **1-9** shows that all penta-coordinate iron complexes have chemically reversible Fe^{II}/Fe^{I} couples, with the exception of some irreversible behavior ($i_{pa}/i_{pc} < 1\pm0.1$) observed for complexes **2** and **8** when cycling at higher scan rates (>100 mV/s). This result indicates that there is a relatively slow geometric reorganization prior to reoxidation for these complexes. Interestingly, DFT calculations on complex **1** indicate that the approximately square-planar Fe(II) complex undergoes a rearrangement to a trigonal-bipyramidal structure upon reduction. Hence, there might be a more hindered (hence slower) rearrangement from square-pyramidal to trigonal-bipyramidal for **2** and **8** compared to the other catalysts investigated here, which would explain the somewhat irreducible behavior of these complexes at higher scan rates. Overpotential values, as determined by comparison to the potential for proton reduction from acetic acid at a platinum electrode (under identical conditions), are observed to vary significantly between different amine substitutions for complexes **1-9**. The most notable differences are seen with more electron donating (R = ^{i}Pr, η = 0.21 – 0.28 V) aliphatic amine substituents and those with more electron withdrawing substituents (R = p-BrC_6H_4, η = 0.09 – 0.16 V), showing a definitive effect of the PNP ligand properties on the metal's redox potential. However, comparison among the complexes with more similar PNP amine substitutions does not show conclusive trends, such as those for R = C_6H_4, p-BrC_6H_4, and p-FC_6H_4, with lower-estimate η values of 0.14, 0.09, and 0.13 V, respectively. In comparison, the 'PCNCP'-type complexes reported by Ott and coworkers have overpotential values ranging from 0.17 to 0.25 V for proton reduction from acetic acid (lower end estimates).[37] Similarly, the 'PCFeCP'-type complex prepared by Jones and coworkers has a reported overpotential range of 0.17 - 0.2 V.[28] The higher overpotentials seen in the 'PCNCP'- and 'PCFeCP'-type complexes suggest that the more rigid, conjugated 'PNP'-type ligand structure

View Article Online
DOI: 10.1039/C5DT03744A

used here is advantageous for lowering the overpotential for proton reduction, and also allows for a stronger amine substituent effect of the phosphine ligand on the metal's redox potential.

Variation in electrocatalytic activity for proton reduction is also seen across our series of compounds, spanning a range of roughly an order of magnitude in TOF with the lowest rate of 0.28 s^{-1} for **8** and the highest TOF of 3.51 s^{-1} for **6**. Direct comparison of similar substituents shows substantial differences, such as the nearly 300% increase in TOF from fluorophenyl (**4**) to fluorobenzyl (**5**), in this example with only the addition of a methylene moiety before the phenyl ring substituent. Similarly, comparing the complexes with the phenyl substituent (**2**) and the butylphenyl substituent (**6**) at the PNP amine shows an increase of more than 200% in TOF (1.58 s^{-1} for (**2**) and 3.51 s^{-1} for (**6**)), which is again thought to be caused by the aliphatic butyl moiety. While this effect could be due to the more electron-donating character of the aliphatic substituent versus the aromatic substituent, the relatively low activity seen in the isopropyl derivative (**1**, 1.38 s^{-1}) does not follow this trend. Alternatively, this might be better attributed to the steric flexibility allowed by the alkyl groups and the geometric structures of the Fe^{II} complexes, as the reduction from Fe^{II} to Fe^{I} very likely causes a change in the geometry of the complexes towards trigonal-bipyramidal (see DFT results above). In this regard, it is interesting to note that complex **1**, which is approximately square planar, shows one of the lowest TOF (and k_{cat}) values, whereas complex **5**, which is already close to trigonal-bipyramidal in its Fe(II) form, has one of the highest catalytic activities. This indicates that the structural rearrangement of the complexes after reduction might be a key factor that determines the electrocatalytic activities of our catalysts. For comparison, 'PCFeCP'-type complex reported by Jones and coworkers, $[Fe(S_2C_6H_4)((C_6H_5)_2P(FeCp_2)P(C_6H_5)_2)(CO)]$, was not seen to reach activity saturation up to a [AcOH] concentration of 1.6 M in THF, with an estimated TOF of 241 s^{-1}, determined by the

View Article Online
DOI: 10.1039/C5DT03744A

same method used here (**equation 1**; catalyst concentration 0.6 mM) at the peak catalytic potential of approximately -1.8 V. Notably, this maximum TOF is nearly two orders of magnitude larger than that of the most active of our compounds (3.51 s^{-1} for **6**), which reach their maximum TOF at much lower acid concentrations.[28]

Bimolecular catalytic rate constants were calculated for **1-9** based on cyclic voltammetry data using equation **2** in an analogous manner to Ott and coworkers. These calculated values also vary widely across the catalyst series by roughly two orders of magnitude, from 8 M^{-1} s^{-1} to 1375 M^{-1} s^{-1}. As expected, the general trend in activity across the series of compounds reported here is preserved in both TOF and rate constant estimates. Interestingly, at peak acid concentrations (0.1 M), a TOF of 137 s^{-1} can be calculated for **6** (**equation 1**), which is over an order of magnitude higher than the TOF calculated for **6** by **equation 2** (3.51 s^{-1}). It is also of interest that the estimated TOFs and the bimolecular rate constants do not correlate with the overpotential in these complexes. The bimolecular rate constants estimated for the corresponding 'PCNCP'-type complex $[Fe(S_2C_6H_4)((C_6H_5)_2PCH_2N(dep)CH_2P(C_6H_5)_2)(CO)]$ by Ott and coworkers is nearly an order of magnitude higher (1000 M^{-1} s^{-1}) as compared to the average k_{cat} value in our series (**Table 1**).[37] The exceptions to this trend are compounds **5** and **6**, which both show exceptional k_{cat} values (1243 and 1375 M^{-1} s^{-1}, respectively) compared to our other complexes. While these k_{cat} values exceed those estimated by Ott and coworkers, comparison of the acid titration CV data shows that our complexes reach activity saturation at much lower acid concentrations (below 0.1 M, with a maximum i_c/i_p of only about 5), whereas for Ott's compound no activity saturation is observed up to an [AcOH] concentration of 0.5 M (resulting in i_c/i_p of approximately 20, and TOF = 77 s^{-1} from **equation 1**). These results show that the bimolecular rate constants are not an accurate predictor of *maximum catalyst activity*, since acid-independent steps in the mechanism

View Article Online
DOI: 10.1039/C5DT03744A

can lead to activity saturation for different catalysts at different acid concentrations, causing substantial differences in maximum TOF values that can be accomplished. The most reasonable explanation for this difference (supported by the DFT results) is that the flexibility afforded from the diphosphines with larger rings may allow for necessary conformational changes to occur more rapidly upon turnover, leading to faster rates for Ott's compounds. The geometric strain observed in the FePNP system is extreme and likely leads to reduced rates and increased ligand lability. In addition, the availability of pendant amines in Ott's complexes that can serve as proton shuttles could contribute to their faster rates. In this regard, DuBois and others have shown that pendant amines can facilitate M-H/H^+ and M/H-H interactions during catalysis, leading to faster catalyst turnover.[9,58-60] On the other hand, comparison of overpotentials shows a distinct advantage of the FePNP unit in our complexes, causing a distinct drop in overpotential as discussed above. This is most pronounced in compound **3** with an E_{cat} of -1.57 V vs. $Fc^{0/+}$, giving an overpotential of only 0.09 V versus platinum. The substantial difference in catalyst stability under turnover, when considered along with the stability of our original catalysts **1**-**9** in solution and in the presence of acid, indicates that the reduced and/or protonated forms of **1**-**9** are significantly less stable than the corresponding intermediates of Ott's catalysts, which are reported to undergo insignificant decomposition over the course of 30 turnovers in slightly over one hour.

Acid titration studies provide insight into the initial steps of catalysis. For all penta-coordinate iron catalysts (**1**-**9**) reported here, protonation did not occur prior to reduction with either acetic or toluenesulfonic acid, as evidenced by solution IR spectroscopy. These results are in contrast to those of Ott and coworkers, who observed blue shifting of the C-O stretching frequency upon addition of TsOH, indicative of ligand protonation as discussed above.[37] This difference, despite

View Article Online
DOI: 10.1039/C5DT03744A

using the same dithiolate ligand as in Ott's complexes, suggests that the PNP ligand structure reported here is structurally unique, and that the amine is generally insufficiently basic to protonate under these conditions (due to resonance stabilization of the amine's lone pair; see Scheme 2). This is further supported by the fact that the potential for electrocatalytic H_2 production is identical to the $E_{1/2}$, the Fe^{II}/Fe^{I} potential in the absence of acid. The mechanism supported by these results therefore proceeds with an initial reduction, followed by protonation. The resulting Fe^{III}-hydride species could either disproportionate to release H_2, or could be further reduced to a Fe^{II}-hydride intermediate. The resulting Fe^{II}-H species could subsequently add a proton to yield H_2 and the original Fe^{II} complex as illustrated below:

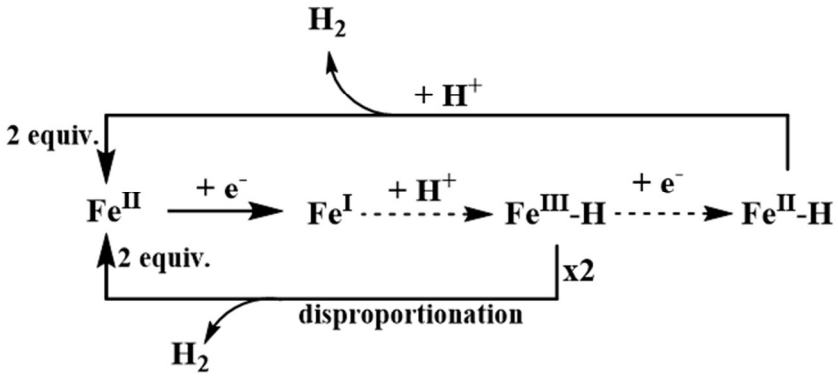

This mechanistic scenario is analogous to mechanistic proposals for proton reduction by cobaloximes.[27,61] In contrast, Ott's complexes have more basic amine sites capable of protonating with stronger acid (TsOH) and potentially accessing an alternative mechanistic pathway with stronger acids. On the other hand, the mechanism proposed for the reaction of their catalysts with the weaker acetic acid follows an identical pathway to that proposed here. Thus, the evidence provided here supports the premise of a common mechanism for dihydrogen production by Fe(PNP) type complexes with weak acids. The more rigid structure of our catalysts leads to very small overpotentials (<100 mV for **3**), and in this way, provides a

View Article Online
DOI: 10.1039/C5DT03744A

guideline of how to improve iron-containing proton reduction catalysts in this regard in the future.

Conclusion

The new penta-coordinate, air-stable iron(II) catalysts reported here all show activity for proton reduction in non-aqueous homogeneous solution, with noticeable variation in activity (TOF = 0.3 - 3.5 s^{-1}; determined by CV) and overpotentials (0.09 - 0.21 V vs. Pt under mildly acidic conditions) upon alteration of the second coordination sphere of the ligand framework. The compounds show some of the lowest overpotentials for proton reduction with mononuclear iron catalysts reported to date. However, this improvement comes at a price of a reduced catalytic rate for the compounds and, unfortunately, a decrease in stability compared to analogous monoiron complexes reported in the literature. The contrast observed here between activity estimates by cyclic voltammetry data and electrolysis illustrates the limitation of activity estimates that are derived under non-turnover conditions (see Supporting Information). Efforts to stabilize catalyst derivatives via use of alternative dithiolate ligands are currently underway. In addition, studies are in progress exploiting the highly functionalizable ligand framework in our catalysts for use in a variety of applications, including surface probes and easily modifiable sensors.

ASSOCIATED CONTENT

Supporting Information. Index of figures, details for overpotential and rate constant calculations, and full crystallographic data sets are available free of charge via the Internet at http://pubs.acs.org

AUTHOR INFORMATION

View Article Online
DOI: 10.1039/C5DT03744A

Corresponding Author

*Nicolai Lehnert: lehnertn@umich.edu

Author Contributions

The manuscript was written through contributions of all authors. All authors have given approval to the final version of the manuscript.

Funding Sources

3M funding (NTFG 5286067 to NL), Rackham Graduate School (University of Michigan)

ACKNOWLEDGMENT

We would like to acknowledge the Rackham Graduate School, University of Michigan, and 3M (NTFG 5286067 to NL) for financial support. We further thank the NSF (grant CHE-0840456) for X-ray instrumentation. The crystal structures of [Fe($S_2C_6H_4$)((C_6H_5)$_2$PN(^{i}Pr)P(C_6H_5)$_2$)CO] (**1**), [Fe($S_2C_6H_4$)((C_6H_5)$_2$PN(p-fluorobenzyl)P(C_6H_5)$_2$)CO] (**5**), and [Co($S_2C_6H_4$)((C_6H_5)$_2$PN(^{i}Pr)P(C_6H_5)$_2$)CO] (**10**) have been deposited in the CCDC under registration numbers 1426274, 1426275 and 1426276.

ABBREVIATIONS

bdt, benzenedithiolate; ^{i}Pr, isopropyl; TBA PF_6: tetrabutylammonium hexafluorophosphate; dep: 1,1-diethoxypropane; Ph: C_6H_5; $FeCp_2$: bis(cyclopentadienyl)iron or ferrocene; Et_3NH BF_4: triethylammonium tetrafluoroborate; TsOH: toluenesulfonic acid

SYNOPSIS A series of penta-coordinate iron complexes with varied 'PNP' diphosphine ligands, [Fe($S_2C_6H_4$)((C_6H_5)$_2$PN(R)P(C_6H_5)$_2$)CO], all air-stable Fe^{II} compounds, show electrocatalytic activity for dihydrogen production at low overpotentials (η = 0.09-0.21 V vs. Pt) with estimated turnover frequencies ranging from 0.3 to 3.5 s^{-1}. Our studies further indicate that these catalysts utilize an EC mechanism, where one-electron reduction triggers protonation and likely formation of a hydride complex in the first step of catalysis.

View Article Online
DOI: 10.1039/C5DT03744A

REFERENCES

(1) Turner, J. A. *Science* **2004**, *305*, 972.
(2) Cammack, R.; Frey, M.; Robson, R. *Hydrogen as a Fuel: Learning from Nature*; Taylor & Francis: London and New York, 2001.
(3) Penner, S. S. *Energy* **2006**, *31*, 33.
(4) McKone, J. R.; Marinescu, S. C.; Brunschwig, B. S.; Winkler, J. R.; Gray , H. B. *Chem. Sci.* **2014**, *5*, 865.
(5) Wang, M.; Chen, L.; Sun, L. *Energy & Environmental Science* **2012**, *5*, 6763.
(6) Helm, M. L.; Stewart, M. P.; Bullock, R. M.; DuBois, M. R.; DuBois, D. L. *Science* **2011**, *333*, 863.
(7) Losse, S.; Vos, J. G.; Rau, S. *Coord. Chem. Rev.* **2010**, *254*, 2492.
(8) Tard, C.; Pickett, C. J. *Chem. Rev.* **2009**, *109*, 2245.
(9) Stewart, M. P.; Ho, M.-H.; Wiese, S.; Lindstrom, M. L.; Thogerson, C. E.; Raugei, S.; Bullock, R. M.; Helm, M. L. *J. Am. Chem. Soc.* **2013**, *135*, 6033.
(10) Eckenhoff, W. T.; Eisenberg, R. *Dalton Trans.* **2012**, *2012*, 13004.
(11) Merki, D.; Fierro, S.; Vrubel, H.; Hu, X. *Chem. Sci.* **2011**, *2*, 1262.
(12) Dey, S.; Rana, A.; Dey, S. G.; Dey, A. *ACS Catalysis* **2013**, *3*, 429.
(13) Canaguier, S.; Artero, V.; Fontecave, M. *J. Chem. Soc. Dalton Trans.* **2008**, 315.
(14) Barton, B. E.; Rauchfuss, T. B. *Inorg. Chem.* **2008**, *47*, 2261.
(15) Zampella, G.; Greco, C.; Fantucci, P.; de Gioia, L. *Inorg. Chem.* **2006**, *45*, 4109.
(16) Yu, Z.; Wang, M.; Li, P.; Dong, W.; Wang, F.; Sun, L. *J. Chem. Soc. Dalton Trans.* **2008**, 2400.
(17) McNamara, W. R.; Han, Z.; Yin, C.-J.; Brennessel, W. W.; Holland, P. L.; Eisenberg, R. *Proc. Natl. Acad. Sci. USA* **2012**, *109*, 15594.
(18) Lakadamyali, F.; Kato, M.; Muresan, N. M.; Reisner, E. *Angew. Chem. Int. Ed.* **2012**, *51*, 9381.
(19) Gao, W.; Ekström, J.; Liu, J.; Chen, C.; Eriksson, L.; Weng, L.; Åkermark, B.; Sun, L. *Inorg. Chem.* **2007**, *46*, 1981.
(20) Duan, L.; Wang, M.; Li, P.; Na, Y.; Wang, N.; Sun, L. *J. Chem. Soc. Dalton Trans.* **2007**, 1277.
(21) Cheah, M. H.; Tard, C.; Borg, S. J.; Liu, X.; Ibrahim, S. K.; Pickett, C. J.; Best, S. P. *J. Am. Chem. Soc.* **2007**, *129*, 11085.
(22) Bigi, J. P.; Hanna, T. E.; Harman, W. H.; Chang, A.; Chang, C. J. *Chem. Commun.* **2010**, *46*, 958.
(23) Baffert, C.; Artero, V.; Fontecave, M. *Inorg. Chem.* **2007**, *46*, 1817.
(24) Pantani, O.; Naskar, S.; Guillot, R.; Millet, P.; Anxolabéhère-Mallart, E.; Aukauloo, A. *Angew. Chem. Int. Ed. Engl.* **2008**, *47*, 9948.
(25) McCrory, C. C. L.; Uyeda, C.; Peters, J. C. *J. Am. Chem. Soc.* **2012**, *134*, 3164.
(26) Hu, X.; Brunschwig, B. S.; Peters, J. C. *J. Am. Chem. Soc.* **2007**, *129*, 8988.
(27) Dempsey, J. L.; Brunschwig, B. S.; Winkler, J. R.; Gray, H. B. *Acc. Chem. Res.* **2009**, *42*, 1995.
(28) Roy, S.; Mazinani, S. K. S.; Groy, T. L.; Gan, L.; Tarakeshwar, P.; Mujica, V.; Jones, A. K. *Inorg. Chem.* **2014**, *53*, 8919.
(29) Berben, L. A.; Peters, J. C. *Chem. Commun.* **2010**, *46*, 398.

View Article Online
DOI: 10.1039/C5DT03744A

(30) Andreiadis, E. S.; Jacques, P.-A.; Tran, P. D.; Leyris, A.; Chavarot-Kerlidou, M.; Jousselme, B.; Matheron, M.; Pecaut, J.; Palacin, S.; Fontecave, M.; Artero, V. *Nat. Chem.* **2013**, *5*, 48.

(31) Carroll, M. E.; Barton, B. E.; Gray, D. L.; Mack, A. E.; Rauchfuss, T. B. *Inorg. Chem.* **2011**, *50*, 9554.

(32) Gärtner, F.; Boddien, A.; Barsch, E.; Fumino, K.; Losse, S.; Junge, H.; Hollmann, D.; Brückner, A.; Ludwig, R.; Beller, M. *Chemistry – A European Journal* **2011**, *17*, 6425.

(33) Rakowski DuBois, M.; DuBois, D. L. *Acc. Chem. Res.* **2009**, *42*, 1974.

(34) Yan, Y.; Xia, B.; Ge, X.; Liu, Z.; Wang, J.-Y.; Wang, X. *ACS Appl. Mater. Interfaces* **2013**, *5*, 12794.

(35) Wouter Maijenburg, A.; Regis, M.; Hattori, A. N.; Tanaka, H.; Choi, K.-S.; ten Elshof, J. E. *ACS Appl. Mater. Interfaces* **2014**, *6*, asap (available online).

(36) Ott, S.; Kritikos, M.; Åkermark, B.; Sun, L.; Lomoth, R. *Angew. Chem. Int. Ed. Engl.* **2004**, *43*, 1006.

(37) Beyler, M.; Ezzaher, S.; Karnahl, M.; Santoni, M.-P.; Lomoth, R.; Ott, S. *Chem. Commun.* **2011**, *47*, 11662.

(38) Wiedner, E. S.; Yang, J. Y.; Dougherty, W. G.; Kassel, W. S.; Bullock, R. M.; DuBois, M. R.; DuBois, D. L. *Organometallics* **2010**, *29*, 5390.

(39) Appel, A. M.; DuBois, D. L.; Rakowski DuBois, M. *J. Am. Chem. Soc.* **2005**, *127*, 12717.

(40) Orthaber, A.; Karnahl, M.; Tschierlei, S.; Streich, D.; Stein, M.; Ott, S. *Dalton Transactions* **2014**, *43*, 4537.

(41) Eady, S. C.; Peczonczyk, S. L.; Maldonado, S.; Lehnert, N. *Chem. Commun.* **2014**, *50*, 8065.

(42) Carroll, M. E.; Barton, B. E.; Rauchfuss, T. B.; Carroll, P. J. *J. Am. Chem. Soc.* **2012**, *134*, 18843.

(43) Stolley, R. M.; Helm, M. L. *Nat Chem* **2014**, *6*, 949.

(44) Le Goff, A.; Artero, V.; Jousselme, B.; Tran, P. D.; Guillet, N.; Métayé, R.; Fihri, A.; Palacin, S.; Fontecave, M. *Science* **2009**, *326*, 1384.

(45) Tran, P. D.; Le Goff, A.; Heidkamp, J.; Jousselme, B.; Guillet, N.; Palacin, S.; Dau, H.; Fontecave, M.; Artero, V. *Angew. Chem. Int. Ed.* **2011**, *50*, 1371.

(46) Blakemore, J. D.; Gupta, A.; Warren, J. J.; Brunschwig, B. S.; Gray, H. B. *J. Am. Chem. Soc.* **2013**, *135*, 18288.

(47) Ibrahim, S. K.; Liu, X.; Tard, C.; Pickett, C. J. *Chem. Commun.* **2007**, 1535.

(48) Liu, G.; Wu, B.; Zhang, J.; Wang, X.; Shao, M.; Wang, J. *Inorg. Chem.* **2009**, *48*, 2383.

(49) Krawicz, A.; Yang, J.; Anzenberg, E.; Yano, J.; Sharp, I. D.; Moore, G. F. *J. Am. Chem. Soc.* **2013**, *135*, 11861.

(50) Nocera, D. G. *Acc. Chem. Res.* **2012**, *45*, 767.

(51) Seo, J.; Pekarek, R. T.; Rose, M. J. *Chem. Commun.* **2015**, *51*, 13264.

(52) Frisch, M. J.; Trucks, G. W.; Schlegel, H. B.; Scuseria, G. E.; Robb, M. A.; Cheeseman, J. R.; Scalmani, G.; Barone, V.; Mennucci, B.; Petersson, G. A.; Nakatsuji, H.; Caricato, M.; Li, X.; Hratchian, H. P.; Izmaylov, A. F.; Bloino, J.; Zheng, G.; Sonnenberg, J. L.; Hada, M.; Ehara, M.; Toyota, K.; Fukuda, R.; Hasegawa, J.; Ishida, M.; Nakajima, T.; Honda, Y.; Kitao, O.; Nakai, H.; Vreven, T.; Montgomery Jr., J. A.; Peralta, J. E.; Ogliaro, F.; Bearpark, M. J.; Heyd, J.; Brothers, E. N.; Kudin, K. N.; Staroverov, V. N.; Kobayashi, R.; Normand, J.;

View Article Online
DOI: 10.1039/C5DT03744A

Raghavachari, K.; Rendell, A. P.; Burant, J. C.; Iyengar, S. S.; Tomasi, J.; Cossi, M.; Rega, N.; Millam, N. J.; Klene, M.; Knox, J. E.; Cross, J. B.; Bakken, V.; Adamo, C.; Jaramillo, J.; Gomperts, R.; Stratmann, R. E.; Yazyev, O.; Austin, A. J.; Cammi, R.; Pomelli, C.; Ochterski, J. W.; Martin, R. L.; Morokuma, K.; Zakrzewski, V. G.; Voth, G. A.; Salvador, P.; Dannenberg, J. J.; Dapprich, S.; Daniels, A. D.; Farkas, Ö.; Foresman, J. B.; Ortiz, J. V.; Cioslowski, J.; Fox, D. J.; Gaussian, Inc.: Wallingford, CT, USA, 2009.

(53) Imhoff, P.; Elsevier, C. J. *J. Organomet. Chem.* **1989**, *361*, C61.

(54) Takács, J.; Markó, L.; Párkányi, L. *J. Organomet. Chem.* **1989**, *361*, 109.

(55) Addison, A. W.; Rao, T. N.; Reedijk, J.; van Rijn, J.; Verschoor, G. C. *J. Chem. Soc., Dalton Trans.* **1984**, 1349.

(56) Costentin, C.; Drouet, S.; Robert, M.; Savéant, J.-M. *J. Am. Chem. Soc.* **2012**, *134*, 11235.

(57) Bard, A. J.; Faukner, L. R. *Electrochemical Methods: Fundamentals and Applications*; 2nd edition ed., 2000.

(58) Rakowski DuBois, M.; DuBois, D. L. *Chem. Soc. Rev.* **2009**, *38*, 62.

(59) Raugei, S.; Chen, S.; Ho, M.-H.; Ginovska-Pangovska, B.; Rousseau, R. J.; Dupuis, M.; DuBois, D. L.; Bullock, R. M. *Chemistry – A European Journal* **2012**, *18*, 6493.

(60) Ezzaher, S.; Capon, J.-F.; Gloaguen, F.; Petillon, F. Y.; Schollhammer, P.; Talarmin, J. *Inorg. Chem.* **2007**, *46*, 9863.

(61) Rose, M. J.; Gray, H. B.; Winkler, J. R. *J. Am. Chem. Soc.* **2012**, *134*, 8310.